ChemPubSoc Europe

DOI: 10.1002/chem.201800631

CHEMISTRY A European Journal Full Paper

Carbon Structures

Polyacrylonitrile-Derived Sponge-Like Micro/Macroporous Carbon for Selective CO_2 Separation

Li-Ping Guo, Qing-Tao Hu, Peng Zhang, Wen-Cui Li, and An-Hui Lu*[a]

Abstract: CO_2 capture under a dynamical flow situation requires adsorbents possessing balanced proportion of macropores as diffusion path and micropores as adsorption reservoir. However, the construction of interconnected micro-/macropores structure coupled with abundant nitrogen species into one carbon skeleton remains a challenge. Here, we report a new approach to prepare sponge-like carbon with a well-developed micro-/macroporous structure and enriched nitrogen species through aqueous phase polymerization of acrylonitrile in the presence of graphene oxide. The tension stress caused by the uniform thermal shrinkage of polyacrylonitrile during the pyrolysis together with the favorable flexibility of graphene oxide sheets are responsible for the formation of the sponge-like morphology. The synergistic effect of micro-/macroporous framework and rich CO_2-philic site enables such carbon to decrease resistance to mass transfer and show high CO_2 dynamic selectivity over N_2 (454) and CH_4 (11), as well as good CO_2 capacity at 298 K under low CO_2 partial pressure (0.17 bar, a typical CO_2 partial pressure in flue gas). The above attributes make this porous carbon a promising candidate for CO_2 capture from flue gas, methane sources and other relevant applications.

Introduction

Carbon dioxide (CO_2) is regarded as a renewable carbon source and a primary contributor to climate change. Thus, its capture from gaseous mixtures such as flue gas (i.e., 5–25 vol.% CO_2) and methane source (i.e., 5–70 vol.% CO_2) is of prime importance.[1] CO_2 capture by means of amine scrubbing is a well-established procedure, but the corrosive nature of the amine and significant energy penalty associated with material regeneration are undesirable. Alternatively, capturing CO_2 by means of pressure, temperature, or a vacuum swing adsorption system as well as the combination of these methods is a good option,[2] for which adsorbents with fast sorption kinetics, high adsorption capacity, good selectivity, and long-term stability under a dynamic flow situation are required.[3]

Promisingly, porous carbons with high surface area, thermal/chemical stability, and hydrophobic surface properties are ideal adsorbents for CO_2 capture.[4] However, the traditional activated carbons always present uncontrolled pore size distributions, and micropores are often not easily accessed due to diffusion limitations for gas molecules. In this case, high equilibrium gas capacity values for an adsorbent will only be an indicator because these could not be achieved under a dynamic flow situation. From the diffusion kinetic point of view, a highly interconnected macroporous structure is required.

In addition, by considering the characteristics of CO_2 molecule, constructing CO_2-philic carbon walls would strengthen interaction of porous carbons towards CO_2 molecules. The introduction of nitrogen species will provide active basic centers, imparting weak chemical interactions with a slightly acidic CO_2 molecule. As a result, CO_2 adsorption capacity and selectivity can be improved significantly.[5] Direct pyrolysis of a nitrogen-containing polymer is a straightforward approach to synthesize nitrogen-containing porous carbons.[6] In this respect, the key step is to design nitrogen-containing polymer with rigid skeleton that can resist structural shrinkage and nitrogen loss during pyrolysis and thus ensure a generation of open and developed porous structure with high residue of nitrogen species. Polyacrylonitrile (PAN) is one of the most suitable candidates for the preparation of nitrogen-containing porous carbons due to its high carbon yield and nitrogen content. Furthermore, PAN can form a molecular ladder configuration through cyclization-aromatization reactions, achieving extra rigidity for the entire structure.[7] However, direct pyrolysis coupled with activation of PAN polymer will only produce microporous nitrogen-containing carbons. Therefore, by keeping the issue of adsorption kinetics in mind and to reach a trade-off between capacity and selectivity of CO_2 adsorbents under a dynamic flow situation,[8] developing porous carbons with interconnected macropores by simultaneously keeping micropores and CO_2-philic nitrogen species stable is highly necessary.

To achieve this goal, we have developed a new method for the preparation of sponge-like nitrogen-enriched carbon by assembly and aqueous phase polymerization of acrylonitrile with graphene oxide sheets. The formation of sponge-like morphology is due to the tension caused by uniform thermal shrinkage

[a] L.-P. Guo, Q.-T. Hu, P. Zhang, Prof. W.-C. Li, Prof. A.-H. Lu
State Key Laboratory of Fine Chemicals, School of Chemical Engineering
Dalian University of Technology, Dalian 116024 (P. R. China)
E-mail: anhuilu@dlut.edu.cn

Supporting information and the ORCID number for the author of this article can be found under https://doi.org/10.1002/chem.201800631.

of PAN during the pyrolysis associated with the favorable flexibility of graphene oxide (GO) sheets together. PAN layers can form a molecular ladder configuration through cyclization-aromatization reactions, which supplies extra rigidity to the entire structure with stable and high content of nitrogen species. Due to the contribution of developed micro-/macroporous structures and nitrogen species dominated surface functionality, this sponge-like porous carbon shows fast diffusion, excellent CO_2 capacity and selectivity, and outstanding reversibility under a dynamic flow situation.

Results and Discussion

Structural features of the synthesized carbon

Sponge-like carbon was prepared by assembly and polymerization of acrylonitrile molecules with GO sheets in aqueous system followed by pyrolysis and activation (Figure 1 a). Here,

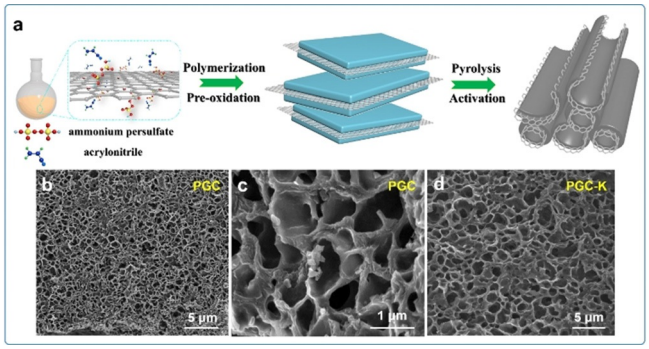

Figure 1. a) Schematic formation of polyacrylonitrile derived sponge-like porous carbon. SEM images of PGC: b) a low magnification overview and c) a high magnification of local structure. d) SEM image of PGC-K.

ammonium persulfate (APS), instead of the often used 2,2-azobisisobutyronitrile (AIBN),[9] as an initiator enabled the in situ free radical polymerization of PAN with GO sheets to occur in an aqueous system, in which the GO sheets can be dispersed more uniformly. SEM images of PGC (Figure 1 b, c) show a well-developed sponge-like macroporous structure which possesses thin walls (≈94 nm) with an interconnected void space of around 500 nm to 1 μm in diameter. By tracking morphology evolution at the different steps of polymerization, pre-oxidation, pyrolysis and activation (Figure S1 a–d in the Supporting Information and Figure 1 b, d), the sponge-like morphology appeared after pyrolysis. In this synthesis, pre-oxidation and pyrolysis of PAN/GO are two key steps. The pre-oxidation process makes the PAN being stably coated on the GO sheets by partial cross-linking and cyclization reactions of PAN side chains.[7] Subsequently, PAN coating layers were bent together with GO sheets due to the thermal-induced tension-stress effect during the pyrolysis process, which was responsible for the formation of a sponge-like macroporous structure. If PAN/GO polymer (Figure S1 a) was directly subjected to activation, skipping over pre-oxidation and pyrolysis steps, or if the oxidized PAN/GO composite (Figure S1 b) was directly subjected to activation, skipping over the pyrolysis step, the obtained samples PG-K and PGO-K could not form the sponge-like macroporous morphology (Figure S1 c, d). This indicates the importance of pre-oxidation and pyrolysis processes on the formation of the rigid carbon skeleton. The present results agree with those in the literature, which show that without pre-oxidation, the yield of carbon is much less and pre-oxidation increases the surface areas of the carbon structure.[10]

The introduction of GO enhances the molecular orientation of the precursor polymer PAN during pre-oxidization and pyrolysis processes by limiting the disorientation of chain segments through π–π interaction.[11] In contrast, the carbon sample prepared in the absence of GO (denoted as PC, Figure S1 e in the Supporting Information) is compacted together, indicating the key role of GO in the formation of the sponge-like macroporous structure. The TEM image (Figure S1 f) shows that PGC has comparatively concentrated micropores and visible graphitic layers. It should be noted that the size of macropores slightly increases after activation (Figure 1 d, PGC-K) due to etching effect of K_2CO_3 over the carbon walls (wall thickness ≈80 nm).

PG-K, PGO-K and PGC-K were subjected to nitrogen sorption analysis to obtain the micropore and mesopore information. All isotherms show steep uptake at relatively low pressure, corresponding to the presence of abundant micropores (Figure 2 a). The PG-K and PGO-K show hysteresis at a relative pressure of >0.4, indicating the presence of a mesoporous structure. The specific surface areas were calculated to be 1994, 1281 and 1143 $m^2 g^{-1}$ for PG-K, PGO-K and PGC-K, respectively (Table 1). As shown in Figure 2 b (inset), the micropore size of PG-K is primarily focused on ≈0.9 nm, whereas the PGO-K has the concentrated micropores of about 0.53 nm. The sample PGC-K with a sponge-like macroporous morphology possesses sharp pore size distribution in the range of 0.68–0.8 nm, the volume of which is approximately 0.23 $cm^3 g^{-1}$, accounting for 50% of its total micropore volume. It is well accepted that the pore size of porous carbon is twice the dynamic diameter of CO_2 (3.3 Å); thus, the CO_2 adsorption potential energy in it will be dramatically enhanced at ambient temperature and pressure.[12]

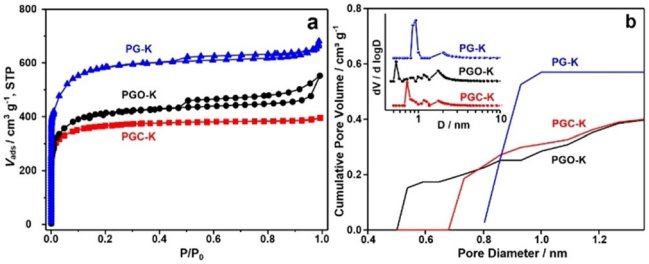

Figure 2. a) N_2 adsorption isotherms of PG-K, PGO-K and PGC-K. b) Cumulative pore volume calculated using the DFT model based upon the adsorption branches and insets of (b) are pore size distributions of PG-K, PGO-K and PGC-K.

Table 1. Summary of structure properties and chemical composition of the porous carbons.

Sample	S_{BET}[a] [$m^2 g^{-1}$]	S_{micro} [$m^2 g^{-1}$]	V_{total}[b] [$cm^3 g^{-1}$]	V_{micro}[c] [$cm^3 g^{-1}$]	D_{peak} [nm]	N [wt%] EA[d]	N [wt%] XPS[e]	CO_2 capacity [mmol g^{-1}] 273 K	CO_2 capacity [mmol g^{-1}] 298 K
PG-K	1994	1920	1.1	0.89	0.90	10.8	7.2	6.5	3.5
PGO-K	1281	831	0.85	0.44	0.53	11.1	8.8	5.4	3.3
PGC-K	1143	861	0.68	0.46	0.73	8.3	6.1	5.6	4.0

[a] S_{BET}: specific surface area calculated by the BET method. [b] V_{total}: total pore volume at $P/P_0 = 0.99$. [c] V_{micro}: micropore volume calculated by t-plot method. [d] EA: elemental analysis. [e] XPS: atomic%.

The nature of the nitrogen species of the porous carbon was investigated by elemental analysis (EA) and X-ray photoelectron spectroscopy (XPS) (Table 1). The nitrogen content of PG-K, PGO-K and PGC-K is 10.8, 11.1 and 8.3 wt%, respectively, and they are significantly greater than those of reported nitrogen-doped porous carbon (e.g., 4.6 wt%).[13] XPS N 1s spectra are deconvoluted to determine the type of the nitrogen species on the surface of the carbon. As shown in Figure 3, the N 1s peak can be deconvoluted into three peaks centered at 398.5, 400.5 and 401.2 eV, representing pyridine N (N-6), pyrrolic N (N-5), and quaternary N (N-Q), respectively.[14] PG-K shows another peak at 403.1 eV, which can be ascribed to the existence of pyridine-*N*-oxide group.[2a] Abundant N-5 and N-6 species on the surface of the carbon provide active basic centers, imparting weak chemical interactions with slightly acidic CO_2 molecules, the mechanism of which accounts for entropic and enthalpic factors.[15]

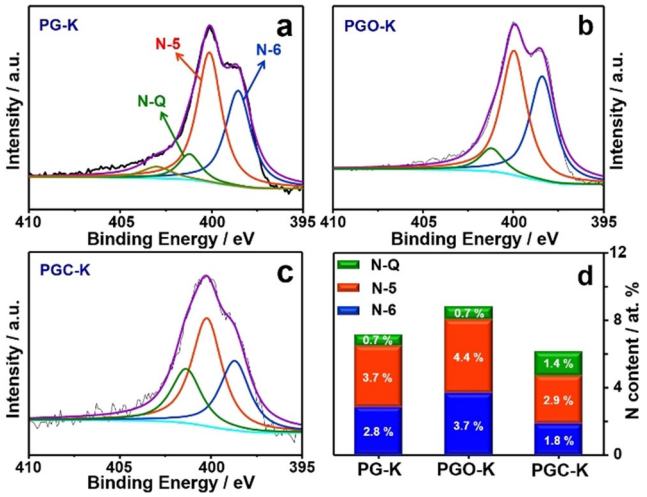

Figure 3. N 1s XPS spectra of a) PG-K, b) PGO-K and c) PGC-K. d) The pyrrolic N (N-5), pyridine N (N-6) and quaternary N (N-Q) species proportion comparison of three samples.

Single-gas equilibrium adsorption and mixed-gas dynamic separation

CO_2 adsorption isotherms of three samples were first studied (Figure 4a, Figure S3a in the Supporting Information). As shown in Figure 4a, CO_2 equilibrium capacities of the samples vary in the range of 3.3–4.0 mmol g^{-1} at 298 K and 1 bar, with

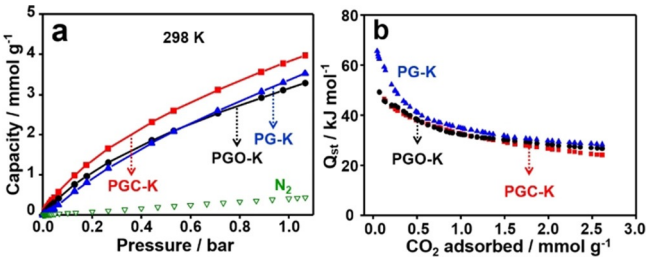

Figure 4. a) CO_2 adsorption isotherms of PG-K, PGO-K and PGC-K at 298 K, N_2 adsorption isotherm (the green line) of PGC-K at 298 K. b) Isosteric heat of adsorption at different CO_2 loadings of PG-K, PGO-K and PGC-K.

the highest adsorption capacity for sample PGC-K. PGC-K exhibits a steady rise in CO_2 capacity over the entire pressure range and reaches the 4.0 mmol g^{-1}, which is higher than those experimental results reported in the literature for porous carbons (Table S2 in the Supporting Information), demonstrating the synergetic effect of three-dimensional macroporous structure for fast molecular diffusion, suitable micropore sizes for enhanced adsorption selectivity and enriched pyrrolic and pyridine nitrogen groups as CO_2-philic sites. In contrast, PGC-K shows a linear isotherm with minor capacity towards nitrogen molecules at 298 K and 1 bar. The preferential adsorption of CO_2 over N_2 arises from a strong dipole-quadrupole interaction between the nitrogen-rich porous carbon and the polarizable CO_2 molecules. It is worth mentioning that the CO_2 capacity of PGO-K (nitrogen content: 11.1 wt%) is slightly higher than that of PG-K (nitrogen content: 10.8 wt%) at low pressure regime (<0.4 bar), illustrating that the nitrogen species plays an important role in this area.[16] The relatively high equilibrium capacity of PG-K comes from the contribution of high specific surface area, and this effect is more significant at 273 K. At 273 K and 1 bar, PG-K adsorbed 6.5 mmol of CO_2 per gram of adsorbent, whereas PGC-K and PGO-K adsorbed up to 5.6 and 5.4 mmol CO_2 per gram adsorbent, respectively. (Figure S3a in the Supporting Information).

The isosteric adsorption heats (Q_{st}) of CO_2 on three samples have been calculated with the Clausius–Claperyron equation from their adsorption isotherms. At the adsorption onset, Q_{st} values of these porous carbon structures are higher than that of pure physical absorption (normally less than 30 kJ mol^{-1}; Figure 4b), the high Q_{st} at low CO_2 loading could be a result of the surface interactions between CO_2 and the basic nitrogen functionalities and/or enhanced fluid–fluid interactions of con-

fined CO_2 in narrow pores.[14b] The characteristic initial sharp decrease to a plateau observed in PG-K curve is indicative of initial adsorption driven by more active basic nitrogen surface sites.[17] Although initial adsorption heat of PG-K is the highest, its low-pressure CO_2 capacity is much lower than the other two samples due to weak adsorption potential between CO_2 molecules and the carbon walls (the micropore size of PG-K is dominantly focused on ≈0.9 nm). The initial adsorption heat of PGC-K is comparable to that of PGO-K and smaller than that of PG-K, but its low-pressure capacity is much higher than the other two samples, demonstrating that the combining effect of three-dimensional macroporous structure, suitable micropore size and enriched pyrrolic and pyridine nitrogen is critical in CO_2 capture. In addition, mild interactions between CO_2 molecules and PGC-K would decrease the cost of regeneration in separation process.

Single-gas equilibrium adsorption results confirm prominent adsorption capacity of PGC-K at ambient conditions. Therefore, PGC-K was directly applied in dynamic breakthrough experiments under conditions that mimic the composition of a flue gas, that is, in a stream of 16.7 vol.% CO_2 balanced with N_2 (Figure 5a) at 298 K and 1.1 bar. N_2 eluted rapidly from the column, while CO_2 was strongly retained. A mass-balance calculation showed that almost no N_2 was adsorbed, whereas 1.03 mmol g^{-1} of CO_2 was adsorbed. Dynamic CO_2 capacity is very close to the equilibrium adsorption value (1.1 mmol g^{-1}) of the single component CO_2 at the partial pressure of 0.17 bar. This implies that CO_2 still preferentially adsorbs onto the adsorbent over N_2, even in a dynamic flow situation. The dynamic selectivity $S_{CO2/N2}$ is estimated to be about 454 for PGC-K, which is much higher than those experimental results reported in the literature for porous carbons (Table S2 in the Supporting Information), MOFs[18] and other adsorbents such as porous organic polymers, [19] zeolite[20] and silica nanoparticles[21] under similar conditions. PGC-K reaches a trade-off between CO_2 capacity and selectivity under a dynamic flow situation due to its interconnected macroporous structure coupled with appropriate micropores and CO_2-philic nitrogen species. In addition, the successive regeneration experiments show that PGC-K retains its CO_2 capacity nicely after 10 cycles (Figure 5b, Figure S3b in the Supporting Information). The moisture has no effect on the separation ability as shown using a $CO_2/H_2O/N_2$ (14/3/83 vol.%) mixture as the feed, indicating good moisture resistance of PGC-K (Figure 5c). The cycling experiments using a $CO_2/H_2O/N_2$ mixture also verify the selective and reversible CO_2 separation performance of PGC-K under moist conditions (Figure 5d).

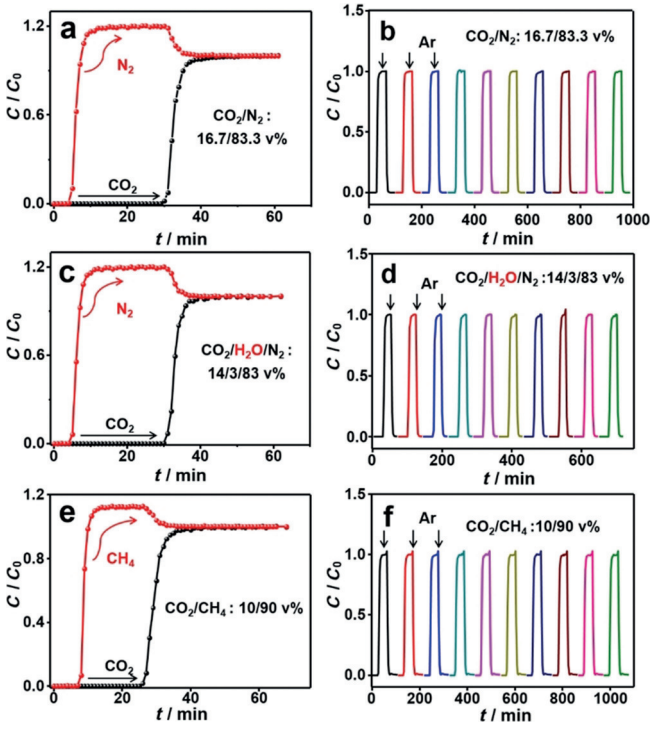

Figure 5. a) Breakthrough curves and b) recycle runs of CO_2 sorption at 298 K, using a stream of 16.7 vol.% CO_2 in N_2; c) breakthrough curves and d) recycle runs of CO_2 sorption at 298 K, using a stream of CO_2/N_2 that is water saturated at 298 K ($CO_2/H_2O/N_2$: 14.0/3.0/83.0 vol.%); e) breakthrough curves and f) recycle runs of CO_2 sorption at 298 K, using a stream of 10 vol.% CO_2 in CH_4. Regeneration was performed by an argon flow (30 mL min^{-1}) at 298 K.

In view of the excellent dynamic CO_2 separation performance of the sponge-like carbon, the separation of CO_2 impurity from methane (CH_4) was also attempted. Dynamic breakthrough curves of PGC-K with a mixed gas stream of CO_2/CH_4 (10/90 vol.%) at 298 K and 1.1 bar (Figure 5e) confirm that the CO_2 adsorption capacity of PGC-K reaches 0.6 mmol g^{-1} and the dynamic selectivity $S_{CO2/CH4}$ is estimated to be 11. It is significantly higher than those previously reported values (generally <5).[22] The enhanced CO_2 separation performance over CH_4 for PGC-K could be attributed to the introduction of polar nitrogen-containing groups that strengthen the intrinsic quadrupole moment of CO_2 molecules, with less impact on the nonpolar CH_4 molecules.[23] Regeneration experiments further indicate a good cyclability of PGC-K (Figure 5f).

Furthermore, by considering the possible application of the sponge-like carbon in pressure swing adsorption technology, the CO_2/N_2 and CO_2/CH_4 separation performance of PGC-K was investigated at the relative high total pressure of 4 bar (Figure S4a,b in the Supporting Information). CO_2 capacity at 298 K rises almost twice from 1.03 to 2.1 mmol g^{-1} as the total pressure increases from 1 to 4 bar due to the existence of interconnected macropores that allow the abundant micropores to be fully accessible. These results would be useful for modeling adsorption separation processes of a fixed-bed sorption.

Generally, there are three different zones existing in the adsorbent bed, that is, the equilibrium zone, mass transfer zone (MTZ) and blank zone (Figure S5 in the Supporting Information). The calculated height of mass transfer zone of adsorption column provides a basis for the scale-up application of PGC-K. Considering that the CO_2 breakthrough curve of PGC-K (Figure 5a) is similar to that of the blank bed (quartz sand) under tested conditions (Figure S4c), it can be deduced that the transfer zone for PGC-K is much shorter. Therefore, the length of the mass transfer zone of PGC-K was calculated based on CO_2 breakthrough curve according to relevant equations listed in in the Supporting Information. The commercial

carbon molecular sieve (CMS-240, pore size: 0.25–0.36 nm) was taken as a reference and its breakthrough curves of CO_2 over N_2 under the same conditions are shown in Figure S4 d. The height of MTZ was calculated as 3.2 cm for PGC-K and 10.7 cm for commercially used carbon molecular sieves. A short mass-transfer zone is helpful to efficiently use the adsorbent bed and reduce the energy cost associated with its subsequent regeneration. These dynamic breakthrough results provide clear evidence that the macropore networks facilitate CO_2 diffusion by reducing the mass-transfer resistance.

Conclusions

We reported a new approach for the preparation of PAN-based porous carbon with sponge-like morphology associated with abundant macropores and micropores. Both pre-oxidation and pyrolysis steps of PAN/GO are crucial for the formation of such structures. This carbon has good CO_2 adsorption capacity due to the synergistic effect of specific porous structure and rich CO_2-philic sites. Importantly, such porous carbon with a macropore network facilitates CO_2 diffusion by reducing the mass-transfer resistance and exhibits high dynamic capacity and selectivity for the capture of CO_2 over N_2 (or CH_4) with good regeneration performance, even in the presence of moisture. The above attributes make this PAN-based carbon a promising candidate for CO_2 capture from flue gas, methane sources as well as other relevant applications.

Experimental Section

Chemicals

The following materials were used as received without further purification. Ammonium persulfate (APS) and potassium carbonate (K_2CO_3) were supplied by Sinopharm Chemical Reagent Co., Ltd. Acrylonitrile (AN) was purchased from Gracia Chemical Technology Co., Ltd. Graphene oxide (GO) colloids used in this work were prepared following a modified Hummers method.[24]

Synthesis of porous carbons

PAN was coated on GO by polymerization of acrylonitrile (AN) using ammonium persulfate (APS) as an initiator. In a typical synthesis, 6 g AN and 180 mg APS (dissolved in 1 mL deionized water) under vacuum in the Schlenk tube were added into 30 mL GO aqueous solution (3 mg mL^{-1}). Subsequently, the obtained black solution was subjected to polymerization in sealed container at 343 K for 7 h. The obtained polymer (PAN/GO polymer) was firstly pre-oxidized by heating in a flow of air at 543 K (oxidized PAN/GO composite) and then pyrolyzed at 1073 K for 2 h under a flow of nitrogen. The obtained carbon sample was named as PGC. For comparison, pure PAN-based carbon (denoted as PC) was prepared following the same synthesis procedure without using GO. To further increase the microporosity, the PAN/GO polymer, oxidized PAN/GO composite and PGC were activated with K_2CO_3 at 973 K for 2 h under a flow of nitrogen. The mass ratio of sample to K_2CO_3 was fixed as 1:1. After that, the activated samples were washed with 0.38 M HCl and water until the filtrates became neutral. The obtained carbons were correspondingly designated as PG-K, PGO-K and PGC-K.

Characterization

Scanning electron microscope (SEM) was carried out with a NOVA NanoSEM 450 instrument. Transmission electron microscopy (TEM) images of samples were obtained with a 200 kV Tecnai G220S-Twin electron microscope equipped with a cold field emission gun. Nitrogen sorption isotherms were measured with an ASAP 2020 sorption analyzer (Micromeritics). Before measurements, carbon samples were degassed under vacuum at 473 K for 4 h. The Brunauer–Emmett–Teller (BET) method was used to calculate the specific surface areas (S_{BET}). Pore size distributions (PSDs) were determined from the adsorption branches of the isotherms using DFT method for micropores and the Barrett–Joyner–Halenda (BJH) model for mesopores. Total pore volumes (V_{total}) were calculated from the amount adsorbed at a relative pressure P/P_0 of 0.99. Micropore volumes (V_{micro}) were calculated using the t-plot method. X-ray photoelectron spectroscopy (XPS) data were obtained with a Thermo VG ESCALAB 250 Microprobe instrument using $Al_{K\alpha}$ radiation as the X-ray source. The binding energy (B.E.) of element was calibrated using a C 1s photoelectron peak at 284.6 eV. Elemental analysis was performed on a CHN elemental analyzer (Vario EL III, Elementar).

Equilibrium adsorption measurements

The gases equilibrium adsorption measurements were performed by using a Micromeritics ASAP 2020 static volumetric analyzer at the required temperature. Prior to each adsorption experiment, samples were degassed for 4 h at 473 K and then cooled down to the required temperature, followed by the introduction of pure gas (N_2 at 99.99%, CH_4 at 99.99% and CO_2 at 99.995% purity) into the system. The gas adsorption capacity in terms of adsorbed volume under standard temperature and pressure (STP) was then recorded. The isosteric heat of adsorption Q_{st} was calculated by using the Clausius–Clapeyron equation: $Q_{st} = RT^2 (\partial \ln P/\partial T)_q$, in which R is the universal gas constant, T is the absolute temperature, P is the equilibrium pressure, and Q is the amount adsorbed.

Dynamic gas separation measurements

The column breakthrough experiments of mixture streams CO_2/N_2 and CO_2/CH_4 (16.7/83.3 and 10/90 *v/v*) were carried out at 298 K and specific pressures in a fixed-bed flow sorber (a stainless-steel tube with an inner diameter of 6.4 mm and the packed length was 120 mm), which were controlled by a pressure controller and a thermostatic water bath, respectively. Thermal pretreatment of sample was conducted at 393 K for 12 h before dynamic adsorption experiments. Adsorbent mass is 2.7 g. The particle size is about 40–60 mesh. The adsorbent bed was first heated at 358 K in Ar at a flow rate of 100 mL min^{-1} for 2 h. Then, breakthrough experiments were performed by switching abruptly from Ar to a gas mixture of CO_2/N_2 or CO_2/CH_4 at a flow rate of 12 mL min^{-1}. A sample saturated with gas molecules was subjected to an Ar flow of 30 mL min^{-1} at 298 K. After 30 min, no gas molecule was detected in the effluent. The effluent gas was monitored online by using an Agilent 7890A gas chromatograph with a thermal conductivity detector (TCD). The blank experiment was conducted at the same temperature and pressure but with a packed bed containing quartz sand.[25]

Acknowledgements

This project was financially supported by National Natural Science Funds of China (21473021), the Cheung Kong Scholars Program of China (T2015036), and the Dalian High-level Personnel of Special Support Program (2015R012).

Conflict of interest

The authors declare no conflict of interest.

Keywords: acrylonitrile · CO_2-selective adsorbent · nitrogen doping · porous carbon

[1] a) K. Huang, C. L. Sun, Z. J. Shi, *Chem. Soc. Rev.* **2011**, *40*, 2435 – 2452; b) Y. B. Wang, Y. M. Wang, W. Z. Zhang, X. B. Lu, *J. Am. Chem. Soc.* **2013**, *135*, 11996 – 12003; c) N. M. Rezayee, C. A. Hu, M. S. Sanford, *J. Am. Chem. Soc.* **2015**, *137*, 1028 – 1031; d) H. Wang, Z. G. Qu, L. Zhou, *J. Membr. Sci.* **2018**, *550*, 448 – 461.

[2] a) M. Sevilla, P. Valle-Vigón, A. B. Fuertes, *Adv. Funct. Mater.* **2011**, *21*, 2781 – 2787; b) J. He, J. W. F. To, P. C. Psarras, H. Yan, T. Atkinson, R. T. Holmes, D. Nordlund, Z. Bao, J. Wilcox, *Adv. Energy Mater.* **2016**, *6*, 1502491.

[3] a) Z. Bao, G. Chang, H. Xing, R. Krishna, Q. Ren, B. Chen, *Energy Environ. Sci.* **2016**, *9*, 3612 – 3641; b) H. Wu, Q. Gong, D. H. Olson, J. Li, *Chem. Rev.* **2012**, *112*, 836 – 868.

[4] a) G. P. Hao, W. C. Li, A. H. Lu, *J. Mater. Chem.* **2011**, *21*, 6447 – 6451; b) A. Stein, Z. Wang, M. A. Fierke, *Adv. Mater.* **2009**, *21*, 265 – 293; c) Q. Wang, J. Luo, Z. Zhong, A. Borgna, *Energy Environ. Sci.* **2011**, *4*, 42 – 55.

[5] a) J. Kou, L. B. Sun, *J. Mater. Chem. A* **2016**, *4*, 17299 – 17307; b) Y. Zhao, X. Liu, K. X. Yao, L. Zhao, Y. Han, *Chem. Mater.* **2012**, *24*, 4725 – 4734.

[6] a) J. H. Lee, N. Park, B. G. Kim, D. S. Jung, K. Im, J. Hur, J. W. Choi, *ACS Nano* **2013**, *7*, 9366 – 9374; b) J. Zhou, Z. H. Li, W. Xing, T. T. Zhu, H. L. Shen, S. P. Zhuo, *Chem. Commun.* **2015**, *51*, 4591 – 4594; c) F. Goettmann, A. Fischer, M. Antonietti, A. Thomas, *Angew. Chem. Int. Ed.* **2006**, *45*, 4467 – 4471; *Angew. Chem.* **2006**, *118*, 4579 – 4583; d) G. P. Hao, W. C. Li, D. Qian, G. H. Wang, W. P. Zhang, T. Zhang, A. Q. Wang, F. Schüth, H. J. Bongard, A. H. Lu, *J. Am. Chem. Soc.* **2011**, *133*, 11378 – 11388; e) S. Wang, W. C. Li, L. Zhang, Z. Y. Jin, A. H. Lu, *J. Mater. Chem. A* **2014**, *2*, 4406 – 4412; f) C. Ge, J. Song, Z. Qin, J. Wang, W. Fan, *ACS Appl. Mater. Interfaces* **2016**, *8*, 18849 – 18859; g) J. Wei, D. Zhou, Z. Sun, Y. Deng, Y. Xia, D. Zhao, *Adv. Funct. Mater.* **2013**, *23*, 2322 – 2328.

[7] a) J. H. Aubert, A. P. Sylwester, *J. Mater. Sci.* **1991**, *26*, 5741 – 5752; b) J. Zhang, X. Pan, Q. Xue, D. He, L. Zhu, Q. Guo, *J. Membr. Sci.* **2017**, *532*, 38 – 46; c) A. G. Sadekar, S. S. Mahadik, A. N. Bang, Z. J. Larimore, C. A. Wisner, M. F. Bertino, A. K. Kalkan, J. T. Mang, C. Sotiriou-Leventis, N. Leventis, *Chem. Mater.* **2012**, *24*, 26 – 47.

[8] X. Cui, R. M. Bustin, G. Dipple, *Fuel* **2004**, *83*, 293 – 303.

[9] L. Yin, J. Wang, F. Lin, J. Yang, Y. Nuli, *Energy Environ. Sci.* **2012**, *5*, 6966 – 6972.

[10] a) S. Mahadik-Khanolkar, S. Donthula, C. Sotiriou-Leventis, N. Leventis, *Chem. Mater.* **2014**, *26*, 1303 – 1317; b) H. M. Far, S. Donthula, T. Taghvaee, A. M. Saeed, Z. Garr, C. Sotiriou-Leventis, N. Leventis, *RSC Adv.* **2017**, *7*, 51104 – 51120.

[11] F. Wu, Y. Lu, G. Shao, F. Zeng, Q. Wu, *Polym. Int.* **2012**, *61*, 1394 – 1399.

[12] a) V. Presser, J. McDonough, S. H. Yeon, Y. Gogotsi, *Energy Environ. Sci.* **2011**, *4*, 3059 – 3066; b) M. Sevilla, J. B. Parra, A. B. Fuertes, *ACS Appl. Mater. Interfaces* **2013**, *5*, 6360 – 6368.

[13] a) S. Xian, F. Xu, Z. Zhao, Y. Li, Z. Li, Q. Xia, J. Xiao, H. Wang, *AIChE J.* **2016**, *62*, 3730 – 3738; b) M. Nandi, K. Okada, A. Dutta, A. Bhaumik, J. Maruyama, D. Derks, H. Uyama, *Chem. Commun.* **2012**, *48*, 10283 – 10285.

[14] a) K. Stanczyk, R. Dziembaj, S. Witkowski, *Carbon* **1995**, *33*, 1383 – 1392; b) J. W. F. To, J. He, J. Mei, R. Haghpanah, Z. Chen, T. Kurosawa, S. Chen, W. G. Bae, L. Pan, J. B. H. Tok, J. Wilcox, Z. Bao, *J. Am. Chem. Soc.* **2016**, *138*, 1001 – 1009.

[15] a) F. Sun, X. Liu, J. X. Pi, L. Wang, Z. Qu, Y. Qin, *J. Mater. Chem. A* **2016**, *4*, 18248 – 18252; b) J. Chen, J. Yang, G. Hu, X. Hu, Z. Li, S. Shen, M. Radosz, M. Fan, *ACS Sustainable Chem. Eng.* **2016**, *4*, 1439 – 1445; c) A. M. Saeed, P. M. Rewatkar, H. M. Far, T. Taghvaee, S. Donthula, C. Mandal, C. Sotiriou-Leventis, N. Leventis, *ACS Appl. Mater. Interfaces* **2017**, *9*, 13520 – 13536.

[16] L. Wang, R. T. Yang, *J. Phys. Chem. C* **2012**, *116*, 1099 – 1106.

[17] a) H. Kim, Y. Kim, M. Yoon, S. Lim, S. M. Park, G. Seo, K. Kim, *J. Am. Chem. Soc.* **2010**, *132*, 12200 – 12202; b) A. Aijaz, N. Fujiwara, Q. Xu, *J. Am. Chem. Soc.* **2014**, *136*, 6790 – 6793.

[18] J. Liu, J. Tian, P. K. Thallapally, B. P. McGrail, *J. Phys. Chem. C* **2012**, *116*, 9575 – 9581.

[19] Y. Zhao, K. X. Yao, B. Teng, T. Zhang, Y. Han, *Energy Environ. Sci.* **2013**, *6*, 3684 – 3692.

[20] M. R. Hudson, W. L. Queen, J. A. Mason, D. W. Fickel, R. F. Lobo, C. M. Brown, *J. Am. Chem. Soc.* **2012**, *134*, 1970 – 1973.

[21] S. M. Rafigh, A. Heydarinasab, *ACS Sustainable Chem. Eng.* **2017**, *5*, 10379 – 10386.

[22] a) S. Duan, M. Gu, X. Du, X. Xian, *Energy Fuels* **2016**, *30*, 2248 – 2256; b) H. Yi, F. Li, P. Ning, X. Tang, J. Peng, Y. Li, H. Deng, *Chem. Eng. J.* **2013**, *215*, 635 – 642; c) J. Wang, R. Krishna, J. Yang, S. Deng, *Environ. Sci. Technol.* **2015**, *49*, 9364 – 9373.

[23] a) Z. Xiang, S. Leng, D. Cao, *J. Phys. Chem. C* **2012**, *116*, 10573 – 10579; b) Y. K. Kim, G. M. Kim, J. W. Lee, *J. Mater. Chem. A* **2015**, *3*, 10919 – 10927.

[24] J. W. S. Hummers, R. E. Offeman, *J. Am. Chem. Soc.* **1958**, *80*, 1339.

[25] N. Álvarez-Gutiérrez, S. Garcia, M. V. Gil, F. Rubiera, C. Pevida, *Energy Fuels* **2016**, *30*, 5005 – 5015.

Manuscript received: February 7, 2018

Accepted manuscript online: March 25, 2018

Version of record online: May 17, 2018